
This copy is for your personal, non-commercial use only.

If you wish to distribute this article to others, you can order high-quality copies for your colleagues, clients, or customers by [clicking here](#).

Permission to republish or repurpose articles or portions of articles can be obtained by following the guidelines [here](#).

The following resources related to this article are available online at www.sciencemag.org (this information is current as of September 29, 2010):

Updated information and services, including high-resolution figures, can be found in the online version of this article at:

<http://www.sciencemag.org/cgi/content/full/309/5738/1236>

A list of selected additional articles on the Science Web sites **related to this article** can be found at:

<http://www.sciencemag.org/cgi/content/full/309/5738/1236#related-content>

This article **cites 29 articles**, 2 of which can be accessed for free:

<http://www.sciencemag.org/cgi/content/full/309/5738/1236#otherarticles>

This article has been **cited by** 31 article(s) on the ISI Web of Science.

This article has been **cited by** 6 articles hosted by HighWire Press; see:

<http://www.sciencemag.org/cgi/content/full/309/5738/1236#otherarticles>

This article appears in the following **subject collections**:

Evolution

<http://www.sciencemag.org/cgi/collection/evolution>

neutron density. The neutron density (n_n) of the source was modeled by solving the simultaneous linear equations describing s -process flow with β^- decay branching to yield

$$\frac{\langle\sigma\rangle N_s)_{186\text{Os}}}{\langle\sigma\rangle N_s)_{188\text{Os}}} = \left(\frac{\lambda_{\beta^-}}{\lambda_{\beta^-} + v_T n_n \langle\sigma\rangle}\right)_{185\text{W}} \times \left(\frac{\lambda_{\beta^-}}{\lambda_{\beta^-} + v_T n_n \langle\sigma\rangle}\right)_{186\text{Re}} \times \prod_{A=185}^{A=188} \left[1 + \frac{1}{\tau_0 \langle\sigma\rangle_{A_i}}\right] \quad (1)$$

where v_T is the thermal neutron velocity, λ is the decay constant, N_s is the s -process abundance, $\langle\sigma\rangle$ is the Maxwellian-averaged neutron capture cross-section, and τ_0 is the average neutron exposure (21). The branching decay of ^{186}Re to ^{186}W by electron capture was neglected for this calculation, because electron capture is diminished at the higher degree of ionization prevailing in stellar interiors (22). Using cross-sections, decay constants, and τ_0 typical of the s process (5, 21, 22), we calculated $^{186}\text{Os}/^{188}\text{Os}$ ratios as a function of stellar neutron density and temperature (Fig. 4). The calculated neutron density for solar s process is similar to that obtained in (21). The $^{186}\text{Os}/^{188}\text{Os} \sim 0.48$ in Tagish Lake Os(i) is matched at stellar neutron densities of 6×10^8 to $10 \times 10^8 \text{ n/cm}^3$.

There are two major neutron sources for the s process produced by helium-burning stellar reactions (α capture): $^{13}\text{C}(\alpha, n)^{16}\text{O}$ and $^{22}\text{Ne}(\alpha, n)^{25}\text{Mg}$. The ^{13}C -source operates at $T \sim 1 \times 10^8 \text{ K}$ and the ^{22}Ne source operates at $T \sim 3 \times 10^8 \text{ K}$ (8, 23). Coupled models of stellar evolution and nucleosynthesis in low-mass asymptotic giant branch stars indicate that during a double neutron pulse the ^{22}Ne source contributes importantly to the abundances of nuclides produced at high neutron densities (up to 10^{10} n/cm^3) (23). This has been identified with the meteoritic Ne-E(H) component (23) and may also contribute the Os(i) component in Tagish Lake. Likely, the main component of s -process Os (and other heavy elements) may be resolved to be a mixture of varied neutron density sources operating in multiple low-mass stars with variable metallicity. Our technique resolved solar s -process Os in primitive chondrites into two components: Os(i) that is likely trapped in SiC grains, and aqua regia-soluble Os that is hosted by other phases (magnetite or Fe sulfides), which provide insights into the galactic chemical evolution of Os. The extractable Os either condensed into acid-soluble minerals from stellar outflows with $\text{C/O} < 1$, or it initially condensed in SiC grains which were then selectively destroyed in the interstellar medium (possibly older grains).

This interpretation—that the anomalous Os isotopic composition in unequilibrated

chondrites results from incomplete access of up to 50 ppm of the total Os present during digestion—has important ramifications to understanding the presence or absence of isotopic anomalies in bulk meteorites for other elements, including Zr, Mo, and Ru (4, 24–29). Because the Os abundance in bulk meteorites is small (≤ 1 ppm) and because Os is one of the first elements to condense, mixing within the solar nebula before condensation into planetesimals must have been extremely efficient in order to result in a homogeneous Os isotopic composition of ± 0.25 epsilon units (i.e., ± 25 ppm) observed in chondrites with greater metamorphic equilibration.

References and Notes

1. E. Zinner, *Annu. Rev. Earth Planet Sci.* **26**, 147 (1998).
2. L. R. Nittler, *Earth Planet. Sci. Lett.* **209**, 259 (2003).
3. M. T. McCulloch, G. J. Wasserburg, *Astrophys. J.* **220**, L15 (1978).
4. Q. Yin, S. Jacobsen, K. Yamashita, *Nature* **415**, 881 (2002).
5. F. Käppeler, R. Gallino, M. Busso, G. Picchio, C. M. Raiteri, *Astrophys. J.* **354**, 630 (1990).
6. E. Anders, N. Grevesse, *Geochim. Cosmochim. Acta* **53**, 197 (1989).
7. H. Palme, H. Beer, *Landolt-Bornstein New Series VI/3a* (Springer-Verlag, Berlin, 1993), pp. 196–221.
8. H. Beer, F. Corvi, P. Mutti, *Astrophys. J.* **474**, 843 (1997).
9. Materials and methods are available as supporting material on Science Online.
10. The traditional normalization to ^{188}Os results in the same systematic differences between the chondrites, but the patterns are shifted and s -process anomalies are obscured because of the relative deficiency of ^{188}Os due to s process.
11. I. Leya, R. Wieler, A. N. Halliday, *Geochim. Cosmochim. Acta* **67**, 529 (2003).
12. T. Nakamura, T. Noguchi, M. E. Zolensky, N. Takaoka, *Lunar Planet. Sci. XXXII*, 1621 (abstr.) (2001).
13. R. J. Walker et al., *Geochim. Cosmochim. Acta* **66**, 4187 (2002).
14. T. K. Croat, F. J. Stadermann, T. J. Bernatowicz, *Lunar Planet. Sci. XXXVI*, 1507 (abstr.) (2005).

15. Y. Kashiv, Z. Cai, B. Lai, S. R. Sutton, R. S. Lewis, A. M. Davis, R. N. Clayton, M. J. Pellin, *Lunar Planet. Sci. XXXII*, 2192 (abstr.) (2001).
16. H. Becker et al., *Lunar Planet. Sci. XXXV*, 1310 (abstr.) (2004).
17. M. M. Grady, A. B. Verchovsky, I. A. Franchi, I. P. Wright, C. T. Pillinger, *Meteorit. Planet. Sci.* **37**, 713 (2002).
18. G. R. Huss, *Nature* **347**, 159 (1990).
19. G. R. Huss, R. S. Lewis, *Geochim. Cosmochim. Acta* **59**, 115 (1995).
20. G. R. Huss, in *Astrophysical Implications of the Laboratory Study of Presolar Materials*, T. J. Bernatowicz, E. Zinner, Eds. (Proceedings of the American Institute of Physics, New York, 1997), vol. 402, pp. 721–748.
21. F. Käppeler, S. Jaag, Z. Y. Bao, G. Reffo, *Astrophys. J.* **366**, 605 (1991).
22. K. Takahashi, K. Yokoi, *Atomic Data Nucl. Data Tables* **36**, 375 (1989).
23. R. Gallino et al., *Astrophys. J.* **497**, 388 (1998).
24. N. Dauphas, B. Marty, L. Reisberg, *Astrophys. J.* **565**, 640 (2002).
25. J. H. Chen, D. A. Papanastassiou, G. J. Wasserburg, H. H. Ngo, *Lunar Planet. Sci. XXXV*, 1431 (abstr.) (2004).
26. D. A. Papanastassiou, J. H. Chen, G. J. Wasserburg, *Lunar Planet. Sci. XXXV*, 1828 (abstr.) (2004).
27. H. Becker, R. J. Walker, *Nature* **425**, 152 (2003).
28. H. Becker, R. J. Walker, *Chem. Geol.* **196**, 43 (2003).
29. M. Schönöbächler et al., *Earth Planet. Sci. Lett.* **216**, 467 (2003).
30. We thank the NASA Cosmochemistry program for funding NAG5-13133 (M.H.), NNG05GB81G (M.H.), and RTOP 344-31-72-06 (A.B.). Samples were obtained from the Field Museum of Natural History, American Museum of Natural History, Museum National d'Histoire Naturelle, Natural History Museum of London, and the Smithsonian Institution. We thank H. Becker and an anonymous reviewer for journal reviews.

Supporting Online Material

www.sciencemag.org/cgi/content/full/309/5738/1233/DC1
 Materials and Methods
 Figs. S1 and S2
 Tables S1 to S4
 References

19 May 2005; accepted 20 July 2005
 10.1126/science.1115053

The Illusion of Invariant Quantities in Life Histories

Sean Nee,^{1*} Nick Colegrave,¹ Stuart A. West,¹ Alan Grafen²

Life-history theory attempts to provide evolutionary explanations for variations in the ways in which animal species live their lives. Recent analyses have suggested that the dimensionless ratios of several key life-history parameters are the same for different species, even across distant taxa. However, we show here that previous analyses may have given a false picture and created an illusion of invariants, which do not necessarily exist; essentially, this is because life-history variables have been regressed against themselves. The following question arises from our analysis: How do we identify an invariant?

Key parameters that determine how species live their lives are the size at which weaning and sexual maturity occur, the number of offspring produced per year, and life span, among others (1–3). A recent approach to understanding the evolution of such life-history parameters has been to show how these analyses can be simplified by examining dimensionless ratios of these parameters, such

as the ratio of offspring weaning weight to maternal weight (1). This approach has been stimulated by analyses that suggest that these dimensionless ratios can be the same for different species, within and even across taxa (Table 1) (1, 4–13). These life-history invariants can be extremely striking, with the regression analyses used to test for them usually explaining 70 to 97% of the variation

in the data. Such strong correlations are exceptional for evolutionary or ecological studies, where the average study explains approximately 5% of the variation in the data (14).

It has been argued that the existence of these invariants implies “symmetry at a deeper level of causal factors” molding life-history evolution (1). Potentially, such invariants, along with other dimensionless ratios that can be derived from them, could underpin the form and shape of the tradeoffs that constrain life-history evolution. Consequently, invariants provide the basis of a unified approach to the study of the evolution of life histories, rather than a mixed basket of species-specific models. This potential importance has led not only to a considerable effort being devoted to measuring these invariants empirically (Table 1) (1, 4–13) but also to a substantial body of theory that attempts to explain their existence and consequences (1, 6, 7, 15–29).

However, we show here that previous analyses may have given a false picture and created an illusion of invariants that do not necessarily exist. We start by considering the clearest case, where one of the variables being examined is necessarily a fraction of the other variable. For example, consider offspring-weaning weight, w , and maternal weight, m , measured for a number of species, with the dimensionless ratio w/m postulated to be an invariant (24, 25, 30). The standard methodology used to test for life-history invariants is to test whether the regression slope of the relationship between $\ln(w)$ and $\ln(m)$ equals 1.0. This is because if the ratio w/m is invariant and equal to some constant c , then a regression of $\ln(w)$ versus $\ln(m)$ would have a slope of 1.0, and an intercept of $\ln(c)$. Although this is true, the converse is not; i.e., a slope of 1.0 does not imply invariance.

Consider the extreme case where the ratio w/m is not invariant and is actually a random variable drawn from a uniform distribution between 0 and 1, which we represent by the variable c . The model is $\ln(w) = \ln(m) + \ln(c)$, which is in the form of a simple linear regression with slope 1.0, $y = x + \epsilon$, where $\ln(c)$ is the non-normally distributed error term ϵ . A regression analysis of data simulated according to this model would return a slope not significantly different from 1.0. Suppose, for the sake of simplicity, that a regression analysis returns a slope of exactly 1.0. Then the R^2 of the regression, which is the proportion of the variation (var) in the dependent variable y , explained by the

variation in the independent variable x , is given by

$$R^2 = \frac{\text{var}[\ln(w)] - \text{var}[\ln(c)]}{\text{var}[\ln(w)]} = \frac{\text{var}[\ln(m)]}{\text{var}[\ln(m)] + \text{var}[\ln(c)]} \quad (1)$$

An example of an analysis performed on simulated data is given in Fig. 1A. This analysis returns a regression slope of 1.0 and an R^2 of 0.94. Figure 1B makes clear that the ratio w/m is far from invariant. Hence, this approach to identifying invariants is invalid.

For this class of so-called invariants, the slope of 1.0 arises because we are, in effect, regressing a variable, X , on X . What accounts for the high R^2 ? When c is drawn from a uniform distribution between 0 and 1, $\ln(c)$ has a variance of 1.0. What accounts for the fact that $\text{var}[\ln(m)] \gg 1.0$? The short answer is that we assumed it does; we simulated data with a variance of 9 (Fig. 1). In real studies, a large variance arises when the data vary over several orders of magnitude; loosely speaking, when the ratio of the largest to the smallest is high. The relationship between orders of magnitude and the variance of a log-normal distribution is as follows. For reasons of familiarity, we will discuss this in terms of \log_{10} transformations. If two data values differ by a factor of 10, an order of magnitude, this is their ratio and it is dimensionless. The value of $\text{var}[\ln(m)]$ is also independent of the scale of measurement. If we plot the logarithmically transformed data, each unit increment on the \log_{10} scale corresponds to a factor of 10. 95% of the data lie between ± 2 SD (σ) of the mean. If on the arithmetic scale, the bulk of the data span M orders of magnitude, then the variance of the data $\sigma^2 \approx (M/4)^2$.

Hence, if m varies over many orders of magnitude, then $\text{var}[\ln(m)] \gg 1.0$, and our R^2 is guaranteed to be high. The most notable invariants are typically taken to be those that hold over several orders of magnitude of variation in the value of the biological characters; we now see that it is this wide variability of the characters that inevitably makes the invariants notable. (The converse also holds: Data that do not span several orders of magnitude may be highly likely to display a slope numerically different from 1.0 and may have a low R^2 .) The R^2 in this particular example would be even higher if we chose values of c from more realistic uniform distributions, such as from the range 0.3 to 1.

The above argument applies to a number of other proposed life-history invariants, where one variable is a simple fraction of the other; for example, size at sex change divided by the maximum body size, or the body size at maturity divided by the maximum asymptotic body size (Table 1).

However, this argument can be readily generalized to other biological variables that involve somewhat more complicated relationships. Consider, for example, the relationship between age at maturity, α , and average adult life span, A , the ratio of which has been argued to be invariant within several taxa (Table 1). Let T be the average total life span of members of a species. Let p be a uniform random number between 0 and 1, so that $\alpha = pT$ and $A = (1 - p)T$, giving

$$\frac{\alpha}{A} = \frac{p}{1 - p} \quad (2)$$

Clearly the ratio α/A is not an invariant. However, our model is again of the form $\ln(\alpha) = \ln(A) + \ln(p) - \ln(1 - p)$, so we expect

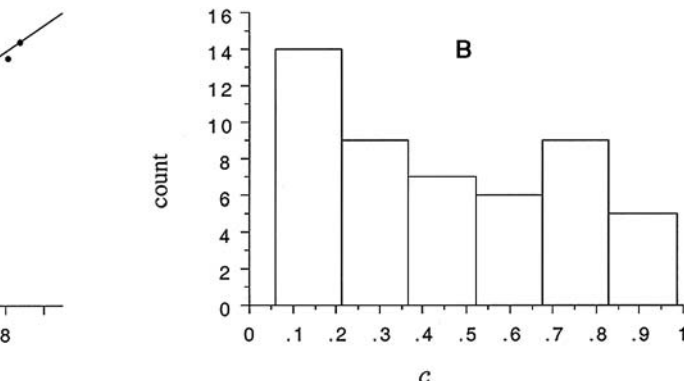
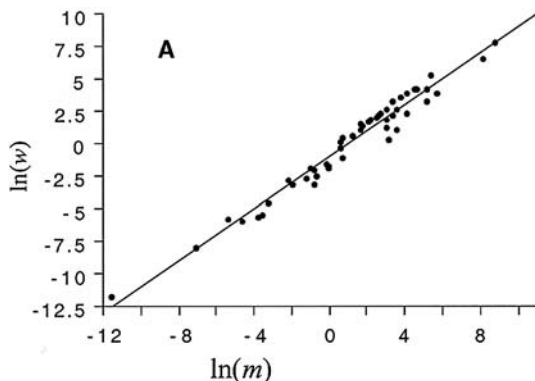
Table 1. Life-history invariants. Shown are some of the dimensionless ratios that have been shown to be life-history invariants, with the use of the regression analysis described in the text.

Dimensionless ratio	Taxa within which invariance has been demonstrated	References
Weaning weight (w)/maternal weight (m)	Mammals	(1, 8, 9)
Average adult life span (A)/age at maturity (α)	Mammals, angiosperms, snakes, lizards, shrimps, nematodes	(1, 6, 10, 11)
Mortality rate (M)/growth coefficient (K)	Fish, shrimps, snakes, lizards, sea urchins, turtles	(1)
Length at maturity (l_α)/maximum asymptotic length (l_∞)	Fish, lizards, snakes	(1, 35)
Yearly fecundity (b) \times age at maturity (α)	Mammals	(1)
Yearly fecundity (b)/mortality rate (M)	Birds, bats	(1, 9, 13)
Maximum asymptotic length (l_∞)/growth coefficient (K)	Fish genera	(1)
Size at sex change (L_{50})/maximum size (L_{\max})	Animals (fish, crustaceans, mollusks, echinoderms)	(4, 7)
Age at sex change (τ)/age at maturity (α)	Fish	(5)
Fraction of body mass to reproduction per unit time (C)/average adult life span (A)	Fish, birds, mammals	(29)

¹Institute of Evolutionary Biology, School of Biological Sciences, University of Edinburgh, West Mains Road, Edinburgh, EH9 3JT, UK. ²Department of Zoology, University of Oxford, South Parks Road, Oxford, OX1 3PS, UK.

*To whom correspondence should be addressed. E-mail: sean.nee@ed.ac.uk

Fig. 1. (A) We randomly generated 50 log-normally distributed maternal weights, m , such that $\ln(m)$ was normally distributed with mean = 2 and SD = 3. This generated a range of weights between 0.001 and just under 7000 units. Because weaning weight, w , must obviously be some fraction of adult body weight, we generated the ratios, c , by drawing 50 random numbers from a uniform distribution between 0 and 1. The figure shows weaning weight plotted against maternal weight on a log-log scale [$\ln(w)$ versus $\ln(m)$]. Regression analysis gives a slope not significantly different from 1, and $R^2 = 0.94$. According to current convention (Table 1), this means that the ratio, c , is invariant. If we repeat



this process 1000 times we get an average R^2 of 0.900 ± 0.001 (SE) with 95% of the runs giving values between 0.799 and 0.957. **(B)** The ratio of weaning weight divided by maternal weight ($c = m/w$) plotted as a histogram. Other random simulations on bounded variables provide similar results (24, 25, 30).

a regression slope of 1.0, because we are regressing X on X , and we expect an R^2 of

$$R^2 = \frac{\text{var}[\ln(A)]}{\text{var}[\ln(A)] + \text{var}[\ln(\frac{p}{1-p})]} \quad (3)$$

Once again, R^2 will be high if A is highly variable.

Some invariants require a moment's reflection before it is seen how they fit into this framework. Consider, for example, the relation between a bird's yearly clutch size, b , and adult mortality rate, M . Suppose that a bird species has E eggs in total over its adult lifetime of Y years; then its yearly clutch size b is E/Y and its annual mortality rate M is $1/Y$. Therefore, $b = ME$, a regression of $\ln(b)$ against $\ln(M)$ is expected to have a slope of 1.0, and

$$R^2 = \frac{\text{var}[\ln(M)]}{\text{var}[\ln(M)] + \text{var}[\ln(E)]} \quad (4)$$

Charnov [table 1.1 and fig. 1.2 in (1)] carries out this regression analysis on data on b and M and finds a slope not significantly different from 1.0. When we compute $E = b/M$ from his tabulated data, we can use the above formula to calculate that the R^2 should be 0.84, which is what Charnov found it to be. More generally, it can be shown that all of the other so-called invariants listed in Table 1 are amenable to the same treatment we have illustrated here.

The studies in Table 1 all explicitly use the regression analysis we have described to demonstrate that a ratio is invariant. From the time of the introduction of invariants, many other studies and discussions have accepted their existence on the basis of these sorts of demonstrations and attempted to explain them theoretically or infer their consequences (6, 15–23, 26, 27). For example, in his review of the canonical monograph on life-history invariants (1), Maynard Smith refers to

the M/b data we have just discussed and says “ M/b is approximately constant (≈ 0.2) for species as different as the tree sparrow and wandering albatross” (31). This is in spite of the fact that the data to which he is referring show the ratio varying between 0.1 and 0.5. Maynard Smith was not the only reviewer to accept that this ratio is constant (32), and the status of these life-history invariants is such that they have now found their way into the popular physics literature (33). In fact, in a population of constant size, the ratio M/b is, essentially, the probability of surviving from egg to breeding age and therefore is constrained to be between 0 and 1.

Given the clear invalidity of using the regression analysis described, a major unresolved problem is how we should search for invariants. One approach that has been suggested is to continue using such analyses, but to compare the R^2 generated by an explicit null model, similar to that used to produce Fig. 1, with that generated by the actual data. Invariance is then accepted if the real data produce an unusually high R^2 (24, 25, 30). However, there is an obvious difficulty with this approach. How does one choose the null model for comparison (25)? In Fig. 1, we used a uniform distribution between 0 and 1, but we could have equally argued for a uniform distribution between, say, 0.5 and 0.9. In addition, the uniformity of the data is not relevant to the question of invariance, because non-uniform distributions can be highly variable, whereas a uniform distribution may have tight bounds. An alternative approach is to examine the covariation between the proposed invariant and other traits considered to be of general importance to life history, such as body size. If covariance is found, the candidate invariant can be rejected (34). However, the lack of any systematic variation in a trait, although it is potentially interesting, is very different from a lack of any variation.

We believe that the best way forward in addressing the existence and importance of invariants is to develop procedures to compare the relative variation in the proposed invariant across species to variation in other scale-free, but not necessarily invariant, measures. If proposed invariants can be expressed in terms of other scale-free measurements, randomization procedures can be used to determine whether the observed values of the invariant are a particularly constrained subset of those that are obtained when the scale-free measurements are allowed to vary independently. Furthermore, this emphasizes that although life-history invariants are often seen as the flagship of the dimensionless approach, the two are in fact separate, and there is no doubt that the dimensionless approach is useful for organizing life histories and looking for general differences across taxa (1, 6, 29). There may even be a benefit to generalizing the study of dimensionless quantities beyond simple ratios to other homogenous functions of degree zero. Although the dimensionless numbers being examined may not be invariant, the mean values may still differ in interesting ways across taxa. For example, the relationship between the age at maturity, α , and the average adult life span, A , groups taxa into poikilothermic indeterminate growers (fish, nematodes, and shrimp), mammals, and birds (1, 10). Such analyses suggest differences that are likely to reflect major differences in the forms of the underlying tradeoffs and open up an array of questions that are more specific (6).

References and Notes

1. E. L. Charnov, *Life History Invariants* (Oxford Univ. Press, Oxford, 1993).
2. S. C. Stearns, *The Evolution of Life Histories* (Oxford Univ. Press, Oxford, 1992).
3. D. A. Roff, *Life History Evolution* (Sinaue, Sunderland, MA, 2002).
4. D. J. Allsop, S. A. West, *J. Evol. Biol.* **16**, 921 (2003).
5. D. J. Allsop, S. A. West, *Nature* **425**, 783 (2003).
6. E. L. Charnov, *Evol. Ecol. Res.* **4**, 749 (2002).

7. E. L. Charnov, U. Skuladottir, *Evol. Ecol. Res.* **2**, 1067 (2000).
8. A. Purvis, P. H. Harvey, *J. Zool.* **237**, 259 (1995).
9. K. E. Jones, A. MacLarnon, *Evol. Ecol. Res.* **3**, 465 (2001).
10. A. W. Gemmill, A. Skorpjng, A. F. Read, *J. Evol. Biol.* **12**, 1148 (1999).
11. S. Morand, *Funct. Ecol.* **10**, 210 (1996).
12. R. E. Willemsen, *J. Zool.* **248**, 379 (1999).
13. R. E. Ricklefs, *Condor* **102**, 9 (2000).
14. A. P. Moller, M. D. Jennions, *Oecologia* **132**, 492 (2002).
15. M. Heino, V. Kaitala, *J. Evol. Biol.* **12**, 423 (1999).
16. N. P. Lester, B. J. Shuter, P. A. Abrams, *Proc. R. Soc. London Ser. B* **271**, 1625 (2004).
17. K. Hawkes, *Nature* **428**, 128 (2004).
18. E. P. Economo, A. J. Kerkhoff, B. J. Enquist, *Ecol. Lett.* **8**, 353 (2005).
19. J. X. He, *Ecology* **82**, 784 (2001).
20. J. Kozłowski, J. Weiner, *Am. Nat.* **149**, 352 (1997).
21. M. Mangel, *Evol. Ecol.* **10**, 249 (1996).
22. A. L. Jensen, *Can. J. Fish. Aquat. Sci.* **53**, 820 (1996).
23. J. R. Beddington, G. P. Kirkwood, *Philos. Trans. R. Soc. London Ser. B* **360**, 163 (2005).
24. P. M. Buston, P. L. Munday, R. R. Warner, *Nature* **428**, 783 (2004).
25. A. Gardner, D. J. Allsop, E. L. Charnov, S. A. West, *Am. Nat.* **165**, 551 (2005).
26. E. H. Williams, K. W. Shertzer, *Can. J. Fish. Aquat. Sci.* **60**, 710 (2003).
27. J. Kozłowski, *Proc. R. Soc. London Ser. B* **263**, 556 (1996).
28. E. L. Charnov, *Nature* **387**, 393 (1997).
29. E. L. Charnov, T. F. Turner, K. O. Winemiller, *Proc. Natl. Acad. Sci. U.S.A.* **98**, 9460 (2001).
30. R. Cipriani, R. Collin, *J. Evol. Biol.* **10.1111/j.1420-9101.2005.00949.x** (2005).
31. J. Maynard Smith, *Q. Rev. Biol.* **68**, 557 (1993).
32. D. B. Miles, *Ecology* **75**, 2143 (1994).
33. G. B. West, J. H. Brown, *Phys. Today* **57**, 36 (2004).
34. J. Clobert, T. Garland, R. Barbaut, *J. Evol. Biol.* **11**, 329 (1998).
35. R. E. Willemsen, A. Hailey, *J. Zool.* **248**, 379 (1999).
36. S.W. is funded by The Royal Society. We are grateful to three anonymous referees, one of whom pointed out the constraint on the *M/b* ratio referred to in the text.

5 May 2005; accepted 4 July 2005
10.1126/science.1114488

Multiple Causes of High Extinction Risk in Large Mammal Species

Marcel Cardillo,^{1,2*} Georgina M. Mace,² Kate E. Jones,^{4,†}
Jon Bielby,² Olaf R. P. Bininda-Emonds,⁵ Wes Sechrest,^{4,‡}
C. David L. Orme,¹ Andy Purvis^{1,3}

Many large animal species have a high risk of extinction. This is usually thought to result simply from the way that species traits associated with vulnerability, such as low reproductive rates, scale with body size. In a broad-scale analysis of extinction risk in mammals, we find two additional patterns in the size selectivity of extinction risk. First, impacts of both intrinsic and environmental factors increase sharply above a threshold body mass around 3 kilograms. Second, whereas extinction risk in smaller species is driven by environmental factors, in larger species it is driven by a combination of environmental factors and intrinsic traits. Thus, the disadvantages of large size are greater than generally recognized, and future loss of large mammal biodiversity could be far more rapid than expected.

A major challenge for conservation biology is to explain why some species are more likely to be threatened with extinction than others (1). One of the traits associated most often with high extinction risk among animal species is large body size (2). In mammals, for example, declining species considered threatened with extinction are an order of magnitude heavier (1374 ± 1.43 g), on average, than nonthreatened species (139 ± 1.13 g) (3). Furthermore, the size selectivity of the current extinction crisis echoes past extinction events such as that

of the late Pleistocene, which disproportionately affected larger species (4, 5). However, it is not clear which mechanisms are primarily responsible for the association between body size and extinction risk (5–9), and a thorough investigation requires large comparative data sets for sizable groups of species spanning a wide range of body sizes. Here, we investigate the association between size and risk with the use of a data set including nearly 4000 species of nonmarine mammals, a group spanning eight orders of magnitude in body mass, from the 2-g least woolly bat to the 4000-kg African elephant.

We used multiple linear regression on phylogenetically independent contrasts (10) to test associations between extinction risk and a range of predictor variables. As our measure of extinction risk, we followed previous studies in the use of classifications based on criterion A of the IUCN Red List (3), converted to a numerical index from 0 to 5 (11–13). This corresponds to a coarse but quantitative measure of the rate of recent and ongoing decline and excludes those threatened species listed simply on the basis of small geographic distribution or population size (3). Potential predictors of extinction risk can be grouped into three broad types: (i) environmental factors, where the size and location of a species'

geographic range determines the environmental features and human impact to which it is exposed; (ii) species' ecological traits, such as population density; and (iii) species' life-history traits, such as gestation length. To represent each of these types, we selected six key predictors [geographic range size, human population density, an index of external threat level, population density, gestation length, and weaning age; see (10) for justification].

Extinction risk shows a positive association with adult body mass [$t = 3.86$, degrees of freedom (d.f.) = 1530, $P = 0.0001$, controlling for geographic range size]. In separate regression models, each key predictor except weaning age is also significantly associated with extinction risk (Table 1). When a term describing the interaction between body mass and the key predictor is added to each model, a significant interaction is found in every case except in the model for geographic range size (Table 1). In every model, the sign of the interaction term indicates that the slope of extinction risk against the key predictor becomes steeper with increasing body mass. The effects of risk-promoting factors on extinction risk, therefore, become stronger as body mass increases.

To visualize the effects of these interactions between body mass and the key predictors on extinction risk, we fitted models within a sliding window with a width of 2 units on the scale of $\ln(\text{body mass})$ and moved the window along the body-mass axis at increments of 0.5 units (Fig. 1). For all predictors, slopes of extinction risk varied substantially along the body-mass axis, confirming the significant body-mass interactions in the regression models. In all cases, there was a sharp increase in slope toward the upper end of the body-mass scale, with steepest slopes found in or near the largest body-mass interval. For weaning age, population density, and external threat, this sharp increase in slope occurs at around 3 kg; for gestation length and geographic range size, it occurs above 20 kg. The slope of extinction risk against human population density increases steadily at smaller body sizes, then drops sharply at around 3 kg, although the steepest positive slope is nevertheless found in the largest body-mass interval (Fig. 1).

¹Division of Biology, Imperial College London, Silwood Park, Ascot SL5 7PY, UK. ²Institute of Zoology, Zoological Society of London, Regent's Park NW1 4RY, UK. ³Natural Environmental Research Council (NERC) Centre for Population Biology, Imperial College London, Silwood Park, Ascot SL5 7PY, UK. ⁴Department of Biology, University of Virginia, Charlottesville, VA 22904–4328, USA. ⁵Lehrstuhl für Tierzucht, Technical University of Munich, Alte Akademie 12, 85354 Freising-Weißenstephan, Germany.

*To whom correspondence should be addressed. E-mail: m.cardillo@imperial.ac.uk

†Present address: Earth Institute, Center for Environmental Research and Conservation, Columbia University, 1200 Amsterdam Avenue, MC5556, New York, NY 10027, USA.

‡Present address: World Conservation Union (IUCN) Global Mammal Assessment, c/o Center for Applied Biodiversity, Conservation International, 1919 M Street N.W., Suite 600, Washington, DC 20036, USA.